

Article

Distributionally Robust Multi-Energy Dynamic Optimal Power Flow Considering Water Spillage with Wasserstein Metric

Gengli Song ^{1,2}  and Hua Wei ^{1,2,*}¹ School of Electrical Engineering, Guangxi University, Nanning 530004, China; glisong@outlook.com² Guangxi Key Laboratory of Power System Optimization and Energy Technology, Guangxi University, Nanning 530004, China

* Correspondence: hweigxu@outlook.com

Abstract: This paper proposes a distributed robust multi-energy dynamic optimal power flow (DR-DOPF) model to overcome the uncertainty of new energy outputs and to reduce water spillage in hydropower plants. The proposed model uses an ambiguity set based on the Wasserstein metric to address the uncertainty of wind and solar power forecasting errors, rendering the model data-driven. With increasing sample size, the conservativeness of the ambiguity set was found to decrease. By deducing the worst-case expectation in the objective function and the distributed robust chance constraints, the exact equivalent form of the worst-case expectation and approximate equivalent form of the distributed robust chance constraints were obtained. The test results of the IEEE-118 and IEEE-300 node systems indicate that the proposed model could reduce water spillage by more than 85% and comprehensive operation cost by approximately 12%. With an increasing number of samples, the model could reduce conservativeness on the premise of satisfying the reliability of safety constraints.



Citation: Song, G.; Wei, H. Distributionally Robust Multi-Energy Dynamic Optimal Power Flow Considering Water Spillage with Wasserstein Metric. *Energies* **2022**, *15*, 3886. <https://doi.org/10.3390/en15113886>

Academic Editors: Zbigniew Leonowicz, Michał Jasiński and Arsalan Najafi

Received: 6 April 2022

Accepted: 12 May 2022

Published: 25 May 2022

Publisher's Note: MDPI stays neutral with regard to jurisdictional claims in published maps and institutional affiliations.



Copyright: © 2022 by the authors. Licensee MDPI, Basel, Switzerland. This article is an open access article distributed under the terms and conditions of the Creative Commons Attribution (CC BY) license (<https://creativecommons.org/licenses/by/4.0/>).

Keywords: multi-energy system; water spillage; distributed robust optimization; Wasserstein; dynamic optimal power flow

1. Introduction

Renewable energy sources, such as hydropower, wind, and solar power, have attracted considerable attention worldwide. Still, the problem of renewable energy power consumption must be solved urgently. The problem of water, wind, and light spillage is very serious, among which water spillage is highly prevalent. Therefore, solving the water spillage problem has become a critical research topic [1]. In addition to poor consumption, the uncertainty of new energy outputs is also an important factor. On the one hand, when dealing with such uncertainty, the traditional dispatching method gives priority to hydropower regulation, which makes for a large regulation burden. On the other hand, the traditional dispatching method is based on the dispatcher's experience in allocating the power imbalance among hydropower plants. Due to the lack of reasonable and accurate planning, this method is prone to improper dispatching, which increases the risk of water spillage. Hence, to solve the water spillage problem, the uncertainty in wind and solar power output must be urgently addressed, and a multi-energy optimal power flow model is needed to fully utilize the characteristics of complementarity and coordination between power plants.

The optimal power flow (OPF) problem has been of concern since it was proposed, and new methods have been proposed in recent years. An enhanced quasi-reflection jellyfish optimization algorithm was proposed in [2] to solve the OPF problem, which performed well and showed resilience in the simulation. An algorithm of social network search optimizers was used for optimal power system operation in [3], and the study in this paper proved that the algorithm has significant stability. An improved heap-based optimization

algorithm was proposed in [4] to address the OPF problem, and its effectiveness and robustness was demonstrated. A multi-objective quasi-reflected jellyfish search optimizer was proposed in [5] to solve the multi-dimensional OPF issue with diverse objectives. The above methods showed good performance in solving OPF problems; however, the uncertainty of new energy outputs was not considered in those models. Therefore, a new OPF model considering the uncertainty of wind and solar power output is needed to reduce water spillage in hydropower plants.

Many advancements have been made in uncertainty research, and effective methods, such as stochastic optimization (SO) [6,7] and robust optimization (RO) [8–10], have been proposed. SO assumes that the considered random variable follows a certain probability distribution, and the original problem is transformed into a deterministic problem through formula deduction [11]. SO requires complete knowledge of the probability distribution information of uncertain parameters, which is usually difficult to obtain in practice. In this case, assuming that the random variable follows a certain probability distribution appears to be too optimistic, which may lead to incorrect decisions. In contrast to SO, RO only needs a sample set of uncertain variables and does not require knowledge of a specific probability distribution. RO limits all possible scenarios of the considered random variables to an uncertain set and then transforms the original problem into a deterministic optimization problem under extreme scenarios. RO can ensure that the constraints are met in the case of absolute risk aversion, but the optimization results are often highly conservative, because this approach ignores the distribution information of uncertain variables.

Distributed robust optimization (DRO) [12] combines the advantages of SO and RO methods. DRO assumes that the real distribution is located within an ambiguity set. DRO does not require knowledge of the specific probability distribution and can effectively overcome the conservativeness of RO. At present, the moment-based ambiguity set is the most widely used option [13–15], i.e., the first- and second-order moments of the probability distribution are used to describe the uncertain set. However, when considering only moment information, the distribution of samples cannot be described in detail, and much probability information is omitted, especially when the number of samples is large. Therefore, this model cannot converge to the real distribution when the sample size approaches infinity.

To overcome this defect, an ambiguity set based on the Wasserstein metric [16,17] was developed. The Wasserstein ambiguity set is a data-driven set. With increasing sample size, the ambiguity set decreases and finally converges to the real distribution. Through research, scholars have made achievements in this area. A distributed robust chance-constrained approximate OPF based on the Wasserstein metric was proposed in [18]. This method employed the distributed robust optimization method of the Wasserstein metric to solve the OPF problem for the first time and used a decoupled linear power flow model to approximate the classical power flow equation. A distributed robust approximation framework of unit commitment based on the Wasserstein metric was developed in [19]. This method obtained an upper approximation of the original problem through mathematical deduction and transformed the original model into a mixed integer linear programming problem. A data-driven distributed robust chance-constrained real-time scheduling model was established in [20], which transformed the original problem into a linear programming problem by linearly reconstructing the secondary generation cost and distributed robust chance constraints. A two-stage distributed robust optimization method was proposed in [21] to address the uncertainty in wind power output in an integrated electric–gas thermal energy system. The above methods have been applied to solve problems of power systems, but research on multi-energy dynamic optimal power flow considering the water spillage of cascade hydropower stations under distributed robust opportunity constraints is lacking.

Accordingly, a distributed robust multi-source dynamic optimal power flow model is proposed in this paper considering abandoned water under the Wasserstein metric. The main contributions are as follows:

(1) Cascade hydropower stations coupled in time and space are introduced into the distributed robust dynamic OPF. The model uses the ambiguity set with the Wasserstein metric to address the uncertainty of wind and solar output. The water spillage cost of hydropower plants is also considered to solve the problem of a large amount of water spillage caused by wind and solar power output uncertainty.

(2) An exact equivalent form of the extreme distribution term in the objective function is obtained via dual reformulation and mathematical deduction. The equivalent form is an affine function of the control variable. The form is concise and the scale remains unchanged with increasing numbers of samples, so this form achieves satisfactory computational performance.

(3) An initial equivalent form is obtained by transforming the distributed robust chance constraint. Although the initial equivalent form is accurate, the number of constraints and variables rapidly increases with an increasing number of samples, resulting in a significant decline in operation efficiency. Therefore, an approximate equivalent model is proposed to overcome the defects. Finally, the original problem is transformed into a mixed-integer linear programming problem, which can be solved efficiently with a commercial solver.

2. Dynamic Optimal Power Flow with Distributed Robust Chance Constraints Based on Wasserstein Metric

2.1. Wasserstein Metric and Ambiguity Set

The ambiguity set based on the Wasserstein metric is constructed as follows:

According to a sampling set of historical data, the empirical distribution can be obtained as $\hat{\mathbb{P}}_N = \frac{1}{N} \sum_{i=1}^N \delta_{\hat{\omega}_i}$, where $\delta_{\hat{\omega}_i}$ is the Dirac measure of $\hat{\omega}_i$ and $\hat{\mathbb{P}}_N$ can be used as an estimate of the real distribution \mathbb{P} . To determine the deviation degree between the constant $\hat{\mathbb{P}}_N$ and the real distribution of \mathbb{P} , the Wasserstein metric is defined as follows:

Let \mathbb{P}_1 and \mathbb{P}_2 be two arbitrary probability distributions. Then, the Wasserstein metric $W : \mathcal{M}(\Xi) \times \mathcal{M}(\Xi) \rightarrow R_+$ is defined as [16]:

$$W(\mathbb{P}_1, \mathbb{P}_2) = \inf_{\Pi} \left\{ \int_{\Xi^2} \|\omega_1 - \omega_2\| \Pi(d\omega_1, d\omega_2) \right\} \tag{1}$$

where $\mathcal{M}(\Xi)$ denotes the set of all probability distributions whose support set is Ξ , Π denotes the joint distribution of ω_1 and ω_2 , $\|\cdot\|$ denotes any norm on \mathbb{R}^m , and $\|\omega_1 - \omega_2\|$ denotes the cost of moving an object of unit mass from distribution \mathbb{P}_1 to \mathbb{P}_2 . Because of its tractability, the L_1 -norm was adopted, and the ambiguity set is defined as:

$$\mathbb{P}_N = \{ \mathbb{P} \in \mathcal{M}(\Xi) \mid W(\hat{\mathbb{P}}_N, \mathbb{P}) < \delta(N) \} \tag{2}$$

The above equation defines a Wasserstein ball with empirical distribution $\hat{\mathbb{P}}_N$ as the center and $\delta(N)$ as the radius, which can be calculated by using the following expression (3) [18]:

$$\delta(N) = C \sqrt{\frac{1}{N} \ln\left(\frac{1}{1-\beta}\right)} \tag{3}$$

where $1 - \beta$ is the confidence level and C is a constant, which can be obtained by solving the following optimization problem:

$$C = 2 \inf_{\eta > 0} \sqrt{\frac{1}{2\eta} \left\{ 1 + \ln \left[\frac{1}{N} \sum_{k=1}^N \exp\left(\eta \|\hat{\omega}_i - \hat{\mu}\|_1^2\right) \right] \right\}} \tag{4}$$

where $\hat{\mu}$ denotes the sample mean value. This equation is a unimodal function of scalar η , which can be solved via the golden section or binary search method.

The ambiguity set based on the Wasserstein metric exhibits the following characteristics: It is a data-driven ambiguity set; with an increasing number of historical samples, the set decreases. When the sample size follows $N \rightarrow \infty$, the radius of the Wasserstein ball converges to 0 and the corresponding ambiguity set converges to the real distribution.

2.2. Power Flow Equation and Its Reformulation

The power flow equation and line power constraints are as follows:

$$\begin{cases} P_i = V_i \sum_{j \in i} V_j (G_{ij} \cos \theta_{ij} + B \sin \theta_{ij}) \\ Q_i = V_i \sum_{j \in i} V_j (G_{ij} \sin \theta_{ij} - B \cos \theta_{ij}) \\ P_{i,j}^l = -V_i^2 g_{ij} + V_i V_j (g_{ij} \cos \theta_{ij} + b_{ij} \sin \theta_{ij}) \end{cases} \quad (5)$$

To deal with fluctuations in wind and solar output, automatic generation control (AGC) is the most widely used scheme in real-world applications. This scheme ensures a real-time power balance of the system by distributing unbalanced wind and photovoltaic power and assigning the unbalanced power to each AGC unit in the form of an affine function. According to the scheme, the actual generating power of each generator unit is:

$$\begin{cases} \tilde{P}_{i,t}^s = -\alpha_{i,t}^s e^T \omega_t + P_{i,t}^s \\ \tilde{P}_{i,t}^h = -\alpha_{i,t}^h e^T \omega_t + P_{i,t}^h \\ \tilde{P}_{i,t}^w = \omega_{i,t} + P_{i,t}^w \\ \tilde{Q}_{i,t} = Q_{i,t} + \sigma \omega_{i,t} \end{cases} \quad (6)$$

where ω_t denotes the vector of the combined forecasting errors of wind and solar power, and $\alpha_{i,t}^s$ and $\alpha_{i,t}^h$ are the participation factors of thermal power units and hydropower units, respectively, satisfying $\sum_{i \in G} \alpha_{i,t}^s + \sum_{i \in H} \alpha_{i,t}^h = 1$, vector $e = [1, 1, \dots, 1]$, and parameter $\sigma = \sin \varphi / \cos \varphi$, where $\cos \varphi$ is the power factor. As the power flow equation (Equation (5)) is nonlinear and cannot be addressed under distributed robust chance constraints, a decoupled linear power flow model [22] was adopted in this paper. According to this model, expressions of the true values of the voltage phase angle, node voltage, and line power can be obtained, as expressed in Equation (7) (the detailed process can be found in [18,22]):

$$\begin{cases} \tilde{\theta}_{it} = -(e^T \omega_t) A_{i \cdot}^\theta (\alpha_t^s + \alpha_t^h) + B_{i \cdot}^\theta \omega_t + \theta_{i,t} \\ \tilde{V}_{it} = -(e^T \omega_t) A_{i \cdot}^v (\alpha_t^s + \alpha_t^h) + B_{i \cdot}^v \omega_t + V_{i,t} \\ \tilde{P}_{k,t}^l = -(e^T \omega_t) A_{i \cdot}^l (\alpha_t^s + \alpha_t^h) + B_{i \cdot}^l \omega_t + P_{k,t}^l \end{cases} \quad (7)$$

where $A^\theta, B^\theta, A^v, B^v, A^l$, and B^l denote the constant coefficient matrices determined by the network parameters, $A_{i \cdot}^\theta$ denotes the vector composed of the elements in the i th row of matrix A^θ , and the other parameters are similar.

2.3. Constraints on Safe Operation and Cascade Hydropower Plants

The safe operation constraint of the power system adopts the following form of distributed robust chance constraints (DRCC):

$$\inf_{\mathbb{P} \in \mathbb{P}_N} \mathbb{P} \{ \underline{V}_i \leq \tilde{V}_{i,t} \leq \bar{V}_i \} \geq 1 - \rho_v \quad (8)$$

$$\inf_{\mathbb{P} \in \mathbb{P}_N} \mathbb{P} \{ \underline{R}_i^s \leq -\alpha_{i,t}^s e^T \omega_t \leq \bar{R}_i^s \} \geq 1 - \rho_r \quad (9)$$

$$\inf_{\mathbb{P} \in \mathbb{P}_N} \mathbb{P} \{ \underline{R}_i^h \leq -\alpha_{i,t}^h e^T \omega_t \leq \bar{R}_i^h \} \geq 1 - \rho_r \quad (10)$$

$$\inf_{\mathbb{P} \in \mathbb{P}_N} \mathbb{P} \{ \underline{P}_i^s \leq P_{i,t}^s - \alpha_{i,t}^s e^T \omega_t \leq \bar{P}_i^s \} \geq 1 - \rho_p \quad (11)$$

$$\inf_{\mathbb{P} \in \mathbb{P}_N} \mathbb{P} \{ \underline{P}_i^h \leq P_{i,t}^h - \alpha_{i,t}^h e^T \omega_t \leq \bar{P}_i^h \} \geq 1 - \rho_p \quad (12)$$

$$\inf_{\mathbb{P} \in \mathbb{P}_N} \mathbb{P} \{ \underline{P}_i^l \leq \tilde{P}_{i,t}^l \leq \bar{P}_i^l \} \geq 1 - \rho_l \quad (13)$$

The above expressions indicate that the probability that the variable matches at least $1 - \rho$ satisfies the corresponding constraints, of which Equation (8) expresses the upper and lower bound constraints of all node voltages, Equations (9) and (10) are the reserve capacity constraints of the generator set, and Equations (11)–(13) are the upper and lower bound constraints of the generator set output and line power.

The constraints of cascade hydropower plants are expressed as follows:

$$\begin{cases} r_{i,t}^h = r_{i-1,t}^h - (q_{i,t} - s_{i,t} + j_{i,t})\Delta t + \tilde{q}_{Ini}\Delta t \\ r_{i0}^h = r_i^{ini}, r_{iT}^h = r_i^{fin}, r_i^h \leq r_{i,t}^h \leq \bar{r}_{i,t}^h \\ q_{i,t} = \sum_{m=1}^M q_{i,m,t} + \underline{q}_{i,m} \\ \bar{q}_{i,m}u_{i,m,t} \leq q_{i,m,t} \leq \bar{q}_{i,m} \\ \bar{q}_{i,m}u_{i,m,t} \leq q_{i,m,t} \leq \bar{q}_{i,m,t}u_{i,m-1,t} \\ P_{i,t} = \sum_{m=1}^M k_{i,m}q_{i,m,t} + P_i^h \end{cases} \quad (14)$$

where $r_{i,t}^h$, $q_{i,t}$, $s_{i,t}$, \tilde{q}_{Ini} , and $j_{i,t}$ denote the storage capacity, power generation flow, water spillage flow, inflow, and natural inflow of reservoir i during period t , respectively, and r_i^{ini} and r_i^{fin} denote the initial and termination storage capacity, respectively. To improve the solution efficiency, the reservoir flow and generation power constraints are approximated with piecewise linear functions, where $q_{i,m,t}$ denotes the flow of the m th segment of hydropower unit i during period t , $k_{i,m}$ and $\bar{q}_{i,m}$ denote the generation power coefficient and upper limit of flow of the m th segment, respectively, $q_{i,t}$ and $P_{i,t}^h$ denote the generation flow and generation power of hydropower unit i during period t , respectively, and $u_{i,m,t}$ is a 0–1 variable. When the flow of hydropower station i during period t exceeds the second segment, the variable is 1; otherwise, it is 0. In addition, there are upper and lower bound constraints and reserve capacity constraints of hydropower stations, which can be expressed in the form of distributed robust opportunity constraints among the safe operation constraints of power systems (Equations (10) and (12)).

2.4. Objective Function and Distributed Robust Optimization Framework

The objective function of this model is to minimize the sum of the actual power generation cost, reserve cost, water spillage cost, and regulation cost of each AGC unit under extreme distribution:

$$\min [\sum_{i \in G} \sum_{t \in T} (FG_i(P_{i,t}^g) + FR_{i,t}) + FS] + \sup_{\mathbb{P} \in \mathbb{P}_N} \mathbb{E}_{\mathbb{P}} (\sum_{i \in G} \sum_{t \in T} \alpha_{i,t}^g d_i^g |e^T \omega_t|) \quad (15)$$

of which:

$$FR_{it} = \bar{c}_i^g \bar{R}_{i,t}^g + \underline{c}_i^g \underline{R}_{i,t}^g + \bar{c}_i^h \bar{R}_{i,t}^h + \underline{c}_i^h \underline{R}_{i,t}^h \quad (16)$$

$$FS = c_s \sum_{i \in H} \sum_{t \in T} s_{i,t} \quad (17)$$

where $FG_i(P_{i,t}^g)$, $FR_{i,t}$, and FS denote the power generation cost, reserve cost, and water spillage cost, respectively. Parameters \bar{c}_i^g , \underline{c}_i^g , and c_s denote the cost coefficient of thermal power, hydropower reserve capacity, and water spillage cost, respectively. Furthermore, d_i^g is the adjustment cost coefficient of the thermal power unit in response to wind and solar forecasting errors. Power generation cost $FG_i(P_{i,t}^g)$ is a nondecreasing quadratic function, which can be approximated with a piecewise linear function to improve calculation efficiency, i.e., $FG_i(P_{i,t}^g)$ can be replaced by decision variables with the following constraints [23]:

$$\Phi_{i,t} \geq k_i^n P_{i,t}^g + b_i^n \quad (18)$$

where k_i^n and b_i^n , respectively, denote the slope and intercept of the n th segment in the piecewise linear approximation of thermal power unit i , which can be determined via the piecewise interpolation method [24]. This objective function can improve not only the

economy but also the feasibility of decisions, as the decisions under this objective function need less adjustment in practice.

The problems involved in this model can be expressed in the following distributed robust optimization framework:

$$\min_x c^T x + \sup_{\mathbb{P} \in \mathbb{P}_N} \mathbb{E}_{\mathbb{P}} \{F(x, \omega)\} \tag{19a}$$

$$s.t. h_i(x) = 0, \tag{19b}$$

$$g_j(x) \geq 0, \tag{19c}$$

$$\sup_{\mathbb{P} \in \mathbb{P}_N} \mathbb{P} \left\{ a_k^T(x) \omega + b_k(x) \leq 0 \right\} \geq 1 - \rho \tag{19d}$$

Optimization problem (19) cannot be solved directly, because the objective function and constraints contain random variables. It must be reformulated and transformed into a deterministic problem with only control variables.

3. Model Reformulation

3.1. Reformulation of The Objective Function

The objective function contains the worst-case expectation. Note that $e^T \omega_t$ is a scalar and appears as a whole in the objective function. Therefore, $\zeta = e^T \omega_t$ is preferable, and its supporting set is $[\underline{\zeta}, \bar{\zeta}]$. Let $(\hat{\zeta}_1, \hat{\zeta}_2, \dots, \hat{\zeta}_N)$ correspond to the sample data $(\hat{\omega}_1, \hat{\omega}_2, \dots, \omega_N)$; then, the worst-case expectation is transformed as follows:

$$\sup_{\mathbb{P} \in \mathbb{P}_N} \mathbb{E}_{\mathbb{P}} \left\{ \sum_{i \in G} \sum_{t \in T} \alpha_{i,t}^s d_i^s |\zeta| \right\} \tag{20}$$

According to [16], Equation (20) can be transformed into the following equation by using a strong duality:

$$\inf_{\kappa \geq 0} \left\{ \kappa \delta + \frac{1}{N} \sum_{i=1}^N \sup_{\underline{\zeta} \leq \zeta \leq \bar{\zeta}} \left[\sum_{i \in G} \sum_{t \in T} \alpha_{i,t}^s d_i^s |\zeta| - \kappa \|\zeta - \hat{\zeta}_i\| \right] \right\} \tag{21}$$

Because problem (21) is an affine function with respect to variable ζ in the interval $[\underline{\zeta}, \hat{\zeta}_i]$ and $[\hat{\zeta}_i, \bar{\zeta}]$, the optimal solution must be obtained at the vertices of the feasible region, i.e., $\underline{\zeta}$, $\hat{\zeta}_i$, or $\bar{\zeta}$. Therefore, the worst-case expectation is equivalent to the following problem:

$$\sup_{\mathbb{P} \in \mathbb{P}_N} \mathbb{E}_{\mathbb{P}} \left\{ \sum_{i \in G} \sum_{t \in T} \alpha_{i,t}^s d_i^s |\zeta| \right\} = \begin{cases} \inf_{\kappa \geq 0} \kappa \delta + \frac{1}{N} \sum_{i=1}^N \eta_i \\ s.t. \eta_i \geq \sum_{i \in G} \sum_{t \in T} \alpha_{i,t}^s d_i^s \bar{\zeta} - \kappa (\bar{\zeta} - \hat{\zeta}_i), \forall i \leq N \\ \eta_i \geq \sum_{i \in G} \sum_{t \in T} \alpha_{i,t}^s d_i^s \underline{\zeta} + \kappa (\underline{\zeta} - \hat{\zeta}_i), \forall i \leq N \\ \eta_i \geq \sum_{i \in G} \sum_{t \in T} \alpha_{i,t}^s d_i^s \hat{\zeta}_i, \forall i \leq N \end{cases} \tag{22}$$

Lemma 1. The optimal value of problem (22) is equal to Equation (23):

$$\sup_{\mathbb{P} \in \mathbb{P}_N} \mathbb{E}_{\mathbb{P}} \left\{ \sum_{i \in G} \sum_{t \in T} \alpha_{i,t}^s d_i^s |\zeta| \right\} = b \sum_{i \in G} \sum_{t \in T} \alpha_{i,t}^s d_i^s \tag{23}$$

where $b = \min \left\{ \max \left\{ \bar{\zeta}, -\underline{\zeta} \right\}, \delta + \sum_{i=1}^N |\hat{\zeta}_k| \right\}$ and δ is the Wasserstein radius. The proof is given in the Appendix A.

Compared with the complex form of the worst-case expectation (Equation (22)), Equation (23) is concise and is only decided by the control variable α in affine form. Therefore, the number of variables and constraints will not increase with an increased number of samples.

3.2. Reformulation of The Distributed Robust Chance

Equations (8)–(13) express the joint distributed robust chance constraint (DRCC). According to [20,25], if the function in the distributed robust chance constraint is affine with respect to both control variable x and random variable ω , i.e., the function exhibits the form of Equation (19d), where $\mathbf{a}_k^T(x)$ is an affine function of x ; then, the DRCC can be transformed into a set as follows:

$$Z = \left\{ x \left| \begin{array}{l} \delta\lambda_k - \rho\beta_k + \frac{1}{N} \sum_{i=1}^N z_i^k \leq 0 \\ \mathbf{a}_k^T(x)\hat{\omega}_i + b_k(x) + \beta_k - z_i^k \leq 0 \\ \|\mathbf{a}_k(x)\|_* \leq \lambda_k \\ \lambda_k, \beta_k, z_i^k \geq 0 \end{array} \right. \right\} \tag{24}$$

Model (24) is an approximate equivalent form of the DRCC with high accuracy, but the number of inequalities and variables in the model can rapidly increase with the number of samples, resulting in a significant decrease in the calculation efficiency of this method when the sample size is large. To overcome this defect, the second equation in Model (24) is substituted into the first one, and the first equation is retained to obtain the approximate set Z_1 of set Z . As the L_1 -norm is used when constructing the ambiguity set, the dual norm $\|\cdot\|_*$ takes the infinite norm L_∞ , and the final approximate set Z_1 is expressed in (25). Compared with set Z , the number of inequalities and variables contained in set Z_1 does not increase with the sample size; therefore, it has better computational performance when dealing with a large sample size.

$$Z_1 = \left\{ x \left| \begin{array}{l} \delta\lambda_k - \rho\beta_k + \frac{1}{N} \sum_{i=1}^N z_i^k \leq 0 \\ \mathbf{a}_k^T(x) \frac{1}{N} \sum_{i=1}^N \hat{\omega}_i + b_k(x) \leq (\rho - 1)\beta_k - \delta\lambda_k \\ -\lambda_k \leq \mathbf{a}_k(x) \leq \lambda_k \\ \lambda_k, \beta_k, z_i^k \geq 0 \end{array} \right. \right\} \tag{25}$$

As such, the difficult part of the original problem is transformed into an easy-to-manage form. The original problem is transformed into a mixed-integer linear programming problem, which can be efficiently solved with a commercial solver.

4. Calculation Results and Discussion

This section presents case studies on modified IEEE-118 and 300 node systems. The 118-node system was used to verify the effectiveness of the proposed DR-DOPF method. The test of the 300-bus system focused on the characteristics of the DR-DOPF method by comparing it to other methods to address the uncertainty. The number of periods of all models was set to 24, and the parameters of wind and solar output data were retrieved from <https://www.tennet.eu/>, accessed on 24 July 2019. The parameters of hydropower stations came from three stations on the Yellow River in China: the Bapanxia, Yanguoxia, and Daxia Hydropower Stations. All the programs were run on a PC with an Intel Core i5 CPU and 8 GB RAM by calling CPLEX with MATLAB 2021a.

4.1. IEEE-118 Node System

4.1.1. Effectiveness Verification

The modified IEEE118 node system includes 16 thermal power plants, three cascade hydropower plants, three wind power plants with a capacity of 200 MW, and two solar power plants with a capacity of 150 MW. The specific parameters of wind and solar power plants are shown in Table 1. To verify the effectiveness of DR-DOPF in reducing the comprehensive power generation cost and water spillage, the scenario displayed in

Figure 1 is selected from the sample. Under this scenario, the real output of the sum of wind and solar power considerably exceeds the forecasted output in periods 5–9 and 15–19.

Table 1. Parameters of wind and solar power.

	Number of Plants	Connection Nodes	Capacity	Power Factor
Wind farm	3	28, 59, 83	200 MW	0.95
Solar power plant	3	36, 74, 97	150 MW	0.95

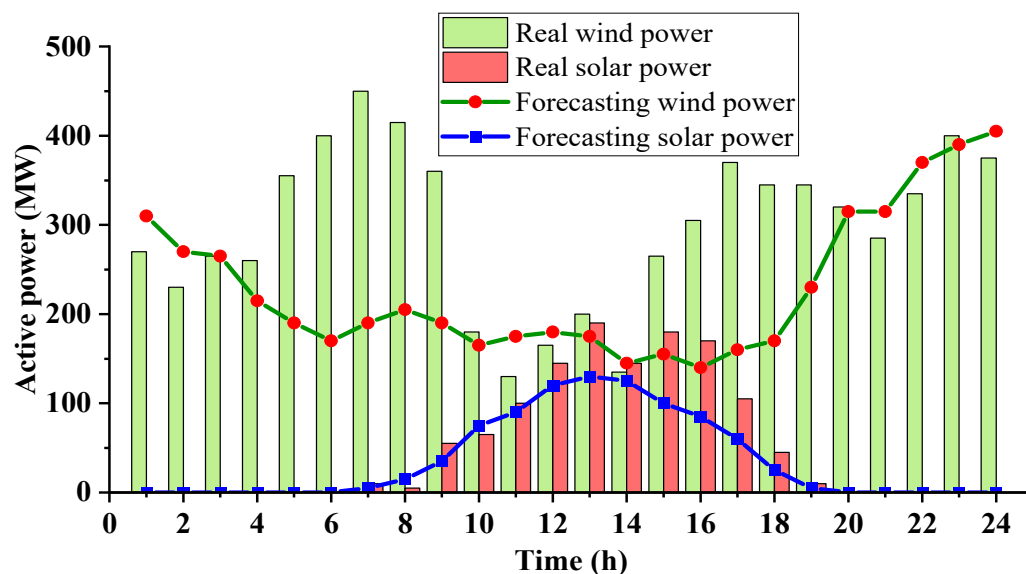


Figure 1. Output of wind and solar power.

For convenience of expression, the traditional dynamic optimal power flow without considering water spillage is abbreviated as TN-DOPF. The TN-DOPF model does not consider the uncertainty of wind and solar output, and the objective function does not include the cost of water spillage. Regarding the DR-DOPF model, the confidence level of the Wasserstein ambiguity set is set to 0.95, and the risk factor is set to $\rho_v = \rho_r = \rho_p = \rho_l = 0.05$.

The result calculated is the day-ahead generation scheduling. To obtain the operation curve and water spillage of hydropower plants in real-time dispatching, the two models are treated as follows.

Regarding the DR-DOPF model, the solution of the real-time output value is given by Equation (6). Specifically, at the real-time dispatching stage, the real output of wind and solar power and the forecasting errors are already known, and the participation factors $\alpha_{i,t}^g$, $\alpha_{i,t}^h$ and the unit planned output $P_{i,t}^g$, $P_{i,t}^h$ are calculated. Hence, the real output of each plant can be directly determined according to Equation (6). Actually, this method dynamically distributes the unbalanced power to each unit according to the participation factor. The flowchart of the DR-DOPF model is shown in Figure 2.

Regarding TN-DOPF, because this model does not involve a participation factor, the actual output cannot be directly determined, but this issue can be addressed according to the actual dispatching situation. To embody the principle by which the dispatcher prioritizes hydropower adjustment in practical operation, it is assumed that 90% of the wind and solar power forecast error is balanced by the hydropower plants and the remaining 10% by the thermal plants, and the power imbalance is assumed to be evenly distributed between the three hydropower plants.

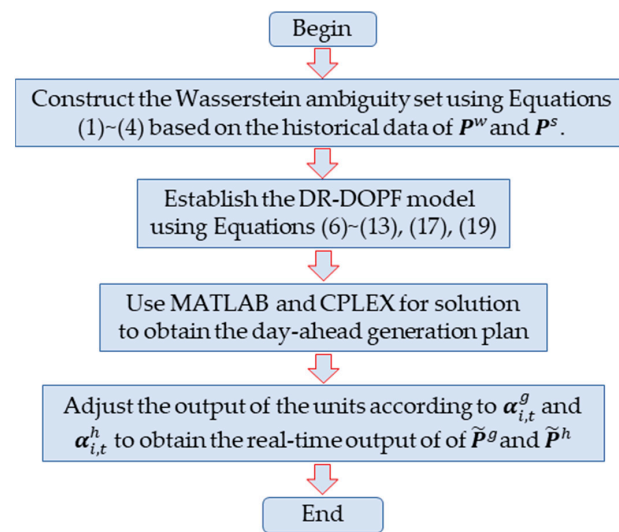


Figure 2. Flowchart of DR-DOPF model.

Figure 3 shows the optimal output of the day-ahead scheduling and the real-time output of the power plant under the DR-DOPF model when the sample size is 100. The real-time output of hydropower and thermal power is lower than that based on the generation plan, because the real output of wind and solar power exceeds the predicted value and the output curve of thermal power is relatively smooth in the previous generation plan but fluctuates in the real-time output curve, especially during periods 5–10 and 15–19. During these two periods, the actual output of wind and solar power is significantly higher than expected, which indicates that the thermal power unit under the DR-DOPF model greatly participates in system power regulation. Although this suggests that the thermal units will produce higher regulation cost, compared to the regulation mode mainly relying on hydropower, the joint optimal regulation mode of hydropower and thermal power can produce higher economic benefits. This point is discussed in detail later.

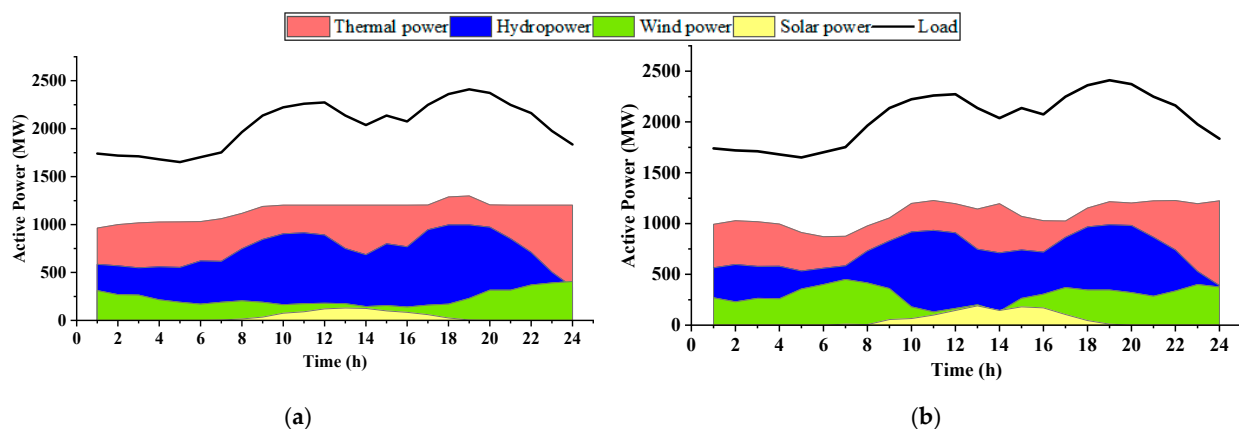


Figure 3. Output of various power plants. (a) Day-ahead scheduling; (b) output of real-time dispatch.

Figure 4 displays the day-ahead and real-time output of hydropower plant 1 under the DR-DOPF and TN-DOPF models; the other two hydropower plants are similar and are not described here. Figure 4a,c reveal that neither model produces water spillage in the day-ahead scheduling. However, at the real-time stage, both models produce water spillage (Figure 4b,d), which is considerably smaller for DR-DOPF than TN-DOPF. The reason is that when dealing with forecasting errors of wind and solar power output, the hydropower plants under these two models must bear a certain amount of the power imbalance. Because the real value of the wind power output during periods 5–9 and 15–19 greatly exceeds

the predicted value, under real-time dispatching, to maintain the system power balance, hydropower plant 1 must greatly reduce the power generation based on the previous power generation plan, resulting in water spillage. In addition, Figure 5 shows that the adjusting power of hydropower plant 1 is lower under the DR-DOPF model than under the TN-DOPF model, especially during periods 5–9 and 15–19; consequently, the water spillage amount under the DR-DOPF model is much smaller.

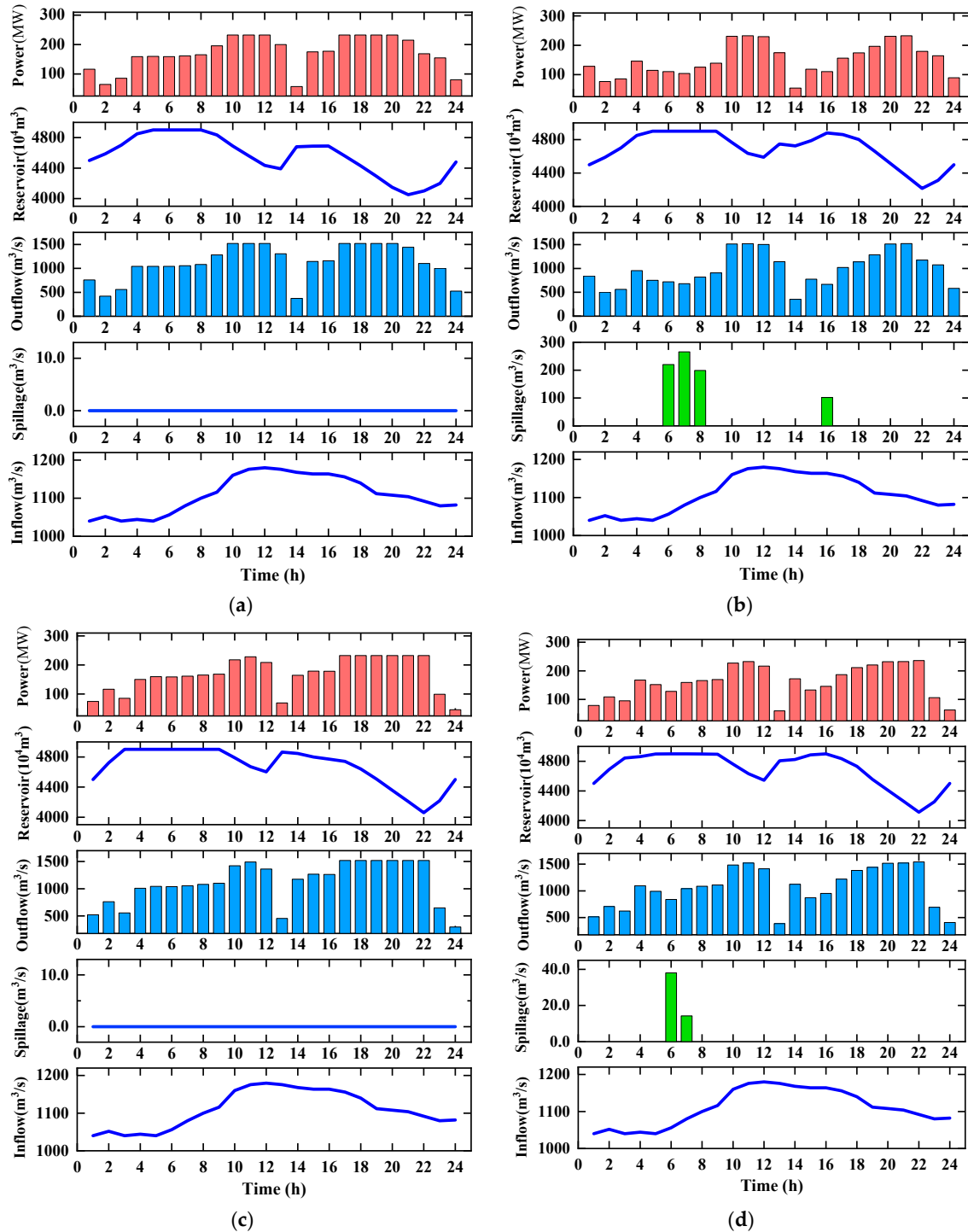


Figure 4. Operation diagram of hydropower plant 1. (a) Day-ahead scheduling of TN-DOPF; (b) real-time output of TN-DOPF; (c) day-ahead scheduling of DR-DOPF; (d) real-time output of DR-DOPF.

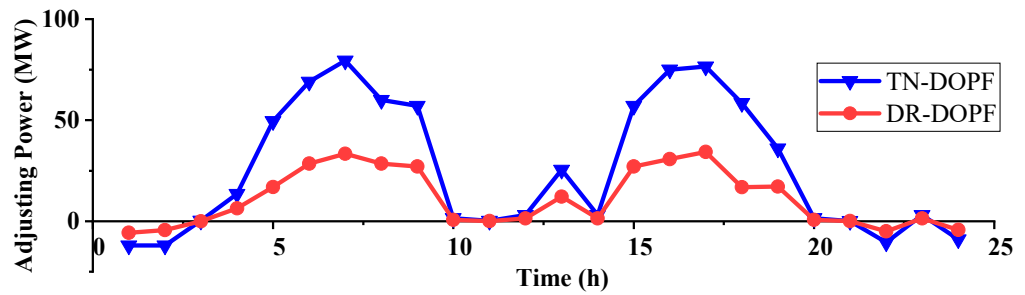


Figure 5. Adjusting power of hydropower plant 1 under two models.

Figure 6 displays the total unbalanced power and adjusting power of thermal power and hydropower under the two models. It can be seen that the adjusting thermal power under DR-DOPF is larger than that of TN-DOPF because it is determined by the participation factors calculated by the day-ahead scheduling. The day-ahead plan considers the uncertainty of wind and solar output, and the objective function contains the water spillage cost. To minimize the water spillage cost, this inevitably requires that the decisions made according to the participation factors can optimally assign the unbalanced power and fully utilize the regulation capacity of the thermal power units. Hence, the regulation burden of the hydropower units can be reduced, and consequently, the water spillage can be decreased. The NDOPF model is modeled on the actual dispatching situation, in which dispatchers tend to prioritize the hydropower plant-adjusting power, and thermal power units participate in regulation to a lesser degree. In this case, power regulation mainly depends on hydropower. Due to the high regulation burden of the hydropower units and the unreasonable distribution of regulation, when the real value of wind and solar power output greatly exceeds the expectation, water spillage easily occurs.

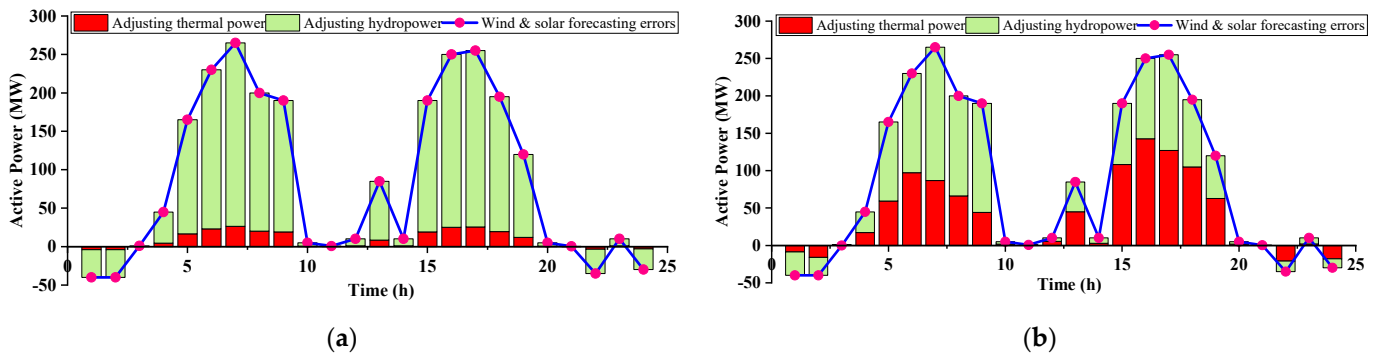


Figure 6. Total adjusting power of thermal power and hydropower with (a) TN-DOPF model and (b) DR-DOPF model.

Under the TN-DOPF model, the proportion of thermal power participating in regulation is low, which can reduce the regulation cost of thermal power units; however, this phenomenon results in large water spillage. Although the water spillage is not reflected in the cost function of TN-DOPF, it cannot be ignored. To fairly compare the comprehensive cost of TN-DOPF and DR-DOPF, the water spillage of TN-DOPF is converted into the water spillage cost according to Equation (17) and added to its objective function value to obtain the comprehensive cost.

Table 2 presents the comprehensive generation cost and total water spillage according to the two methods. Compared with the TN-DOPF model, the total water spillage of DR-DOPF decreases considerably, with a decrease ratio of more than 86%, and the comprehensive cost decreases by more than 12%, which indicates that this model can effectively reduce the total water spillage and comprehensive generation cost. This analysis confirms the previous conclusion that the joint optimal regulation of hydropower and thermal power

can produce higher comprehensive economic benefits compared to regulation mainly relying on hydropower.

Table 2. Comparison of TN-DOPF and DR-DOPF results.

Model	Comprehensive Cost		Total Water Spillage	
	Value ($\times 10^5$ USD)	Reduction Ratio	Value ($\times 10^5$ m ³)	Reduction Ratio
NDR-DOPF	2.830	–	69.746	–
DR-DOPF	2.473	12.6%	9.275	86.7%

Table 3 summarizes the test results of DR-DOPF for various sample sizes. The Wasserstein radius exhibits a negative correlation with sample size, because when more sample data are used, more sufficient information can be obtained about the real probability distribution. Therefore, impossible distributions can be excluded from the Wasserstein ball, resulting in a narrower radius range, less conservativeness of the ambiguity set, and a lower comprehensive cost and water spillage. It can be seen that when the sample size increases from 20 to 5000, the comprehensive power generation cost of the system reduces from 2.613×10^5 USD to 2.409×10^5 USD, a reduction of 7.8%; and total water spillage reduces from 9.458×10^5 m³ to 9.201×10^5 m³, a reduction of 2.7%. This result verifies that with the increase in the sample size, the conservatism of the model lessens and the economy of the model improves. In addition, it should be noted that the number of constraints and variables of DR-DOPF do not increase with the sample size, and the operation time basically remains stable from 28–30 s, which indicates that the DR-DOPF model achieves good computational performance.

Table 3. Test results of DR-DOPF under various sample numbers.

Sample Size	$\delta(N)$	Number of Constraints	Number of Variables	CPU Time (s)	Comprehensive Cost ($\times 10^5$ USD)	Total Water Spillage ($\times 10^5$ m ³)
20	9.731	7341	34,806	29.2	2.613	9.458
50	3.406	7341	34,806	28.6	2.518	9.326
200	1.557	7341	34,806	28.3	2.448	9.238
1000	0.348	7341	34,806	29.7	2.418	9.217
2000	0.102	7341	34,806	29.1	2.409	9.201

4.1.2. Comparisons with RO and SO

In this part, the characteristics of the DR-DOPF method and RO and SO are evaluated. The RO model requires that safety constraints (8–13) must be satisfied in any case. The SO method assumes that samples obey a normal distribution [26,27]. In this case, constraints (8–13) can be transformed into second-order cone constraints [28]. The calculation results obtained using these methods are displayed in Figure 7.

Figure 7 shows that the RO method has the largest water spillage and comprehensive cost, and the SO method has the smallest. Regardless of the sample size, the water spillage and comprehensive cost of DR-DOPF always vary between RO and SO because RO completely ignores the distribution information of samples and is too conservative, and SP assumes that the sample follows a certain distribution, which is too aggressive, while DR-DOPF completely depends on the obtained samples. When limited samples are used, the corresponding Wasserstein radius is large. The extreme distribution in the ambiguity set deviates considerably from the real distribution, so the calculation result is relatively conservative, and is closer to RO at this stage. When the sample size increases, the ambiguity set shrinks, and the extreme distribution is closer to the real distribution. Therefore, the conservatism of the calculation result decreases, and the result is closer to SP. In summary, the order of conservatism from high to low is RO > DR-DOPF (20) > DR-DOPF (50) > DR-DOPF (200) > DR-DOPF (1000) > DR-DOPF (2000) > SO.

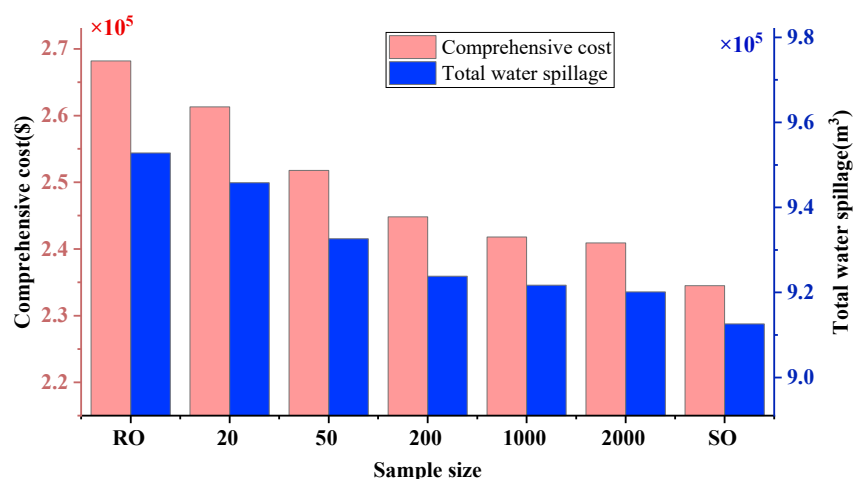


Figure 7. Test results under DR-DOPF, RO, and SO methods.

4.2. IEEE-300 Node System

The modified IEEE-300 system includes 30 thermal power plants, among which the parameters of cascade hydropower stations, wind farms, and photovoltaic power plants are the same as those of the 118-node system, and the scenario shown in Figure 1 is still selected as the scenario of wind and solar output. The wind farms are connected on bus 77, 186, and 235 respectively, and the solar power plants are connected on bus 49, 123, and 284, respectively. DR-DOPF, RO, and SO results are obtained on the same sample set. In addition, the Monte Carlo simulation method is applied, involving 10^4 samples, to evaluate the performance beyond the sample, i.e., the minimum reliability of all security constraints.

4.2.1. Effectiveness Verification

Similar to the method of node 118, in this part, we first compare the test results of DR-DOPF and TN-DOPF models to verify the effectiveness of the proposed DR-DOPF model in reducing the comprehensive power generation cost and water spillage. The results are shown in Table 4.

Table 4. Comparison of TN-DOPF and DR-DOPF results.

Model	Comprehensive Cost (USD)		Total Water Spillage (m³)	
	Value ($\times 10^5$ USD)	Reduction Ratio	Value ($\times 10^5$ m³)	Reduction Ratio
TN-DOPF	6.035	–	53.154	–
DR-DOPF	5.341	11.5%	6.219	88.3%

Table 4 presents the test results of TN-DOPF and DR-DOPF when the sample size is 100. Compared with TN-DOPF, the total water spillage of DR-DOPF decreases considerably, with a decrease ratio of more than 88%, and the comprehensive cost decreases by approximately 12%. The results of the IEEE-300 node system indicate that the proposed DR-DOPF model can reduce the comprehensive generation cost and water spillage effectively. This conclusion is similar to that for the 118-node system.

4.2.2. Comparisons with RO and SP

Table 5 summarizes the comparison test results of the DR-DOPF model with RO and SO methods using various sample sizes, where the confidence level of the Wasserstein ambiguity set is set to 0.95, the risk factor is set to $\rho_v = \rho_r = \rho_p = \rho_l = 0.05$, and the processing method of RO and SO is the same as that of the IEEE118 node.

Table 5. Comparison of the DR-DOPF, RO, and SP results.

Model	Sample Size	Comprehensive Cost ($\times 10^6$ USD)	Total Water Spillage ($\times 10^5$ m ³)	CPU Time (s)	Reliability (%)
DR-DOPF	20	5.468	6.338	47.2	99.98
	50	5.379	6.247	48.6	99.56
	200	5.323	6.195	47.7	99.18
	1000	5.291	6.162	46.2	98.86
	2000	5.276	6.147	48.5	98.52
RO	2000	5.540	6.416	18.3	100
SO	2000	5.198	6.039	27.9	93.14

As can be seen from Table 5, the results of the IEEE-300 node system are similar to those of the IEEE-118 system. Specifically, RO has the highest comprehensive generation cost and total water spillage, SO has the lowest, and the value of DR-DOPF is always between RO and SO and decreases with the sample size. In terms of the calculation time, DR-DOPF requires the longest time, followed by SO, and RO requires the shortest time. When the sample size increases, the calculation time of DR-DOPF basically remains unchanged because the number of constraints and variables do not change with the number of samples; therefore, the computational burden basically remains constant.

Table 5 also compares the reliability levels of the safety constraints of the three methods. RO exhibits the highest reliability of 100%, but obtaining high reliability has drawbacks; notably, the comprehensive cost and total water spillage of RO are the highest in all cases. In other words, the RO model is the most conservative. SO attains the lowest reliability and does not satisfy 95% of the minimum reliability requirements of the safety constraints. This occurs because SO assumes that the sample follows a certain distribution (normal distribution). However, the real distribution of the prediction error may not follow a normal distribution [29,30], which results in an over-aggressive strategy; therefore, it does not satisfy the minimum reliability requirements. The reliability of DR-DOPF lies between RO and SO, which can satisfy the minimum requirements of reliability. With an increasing number of samples, the reliability of the DR-DOPF model gradually decreases. This occurs because with increased samples, the Wasserstein ambiguity set decreases, which reduces the conservativeness of the DR-DOPF model and the comprehensive cost and reliability. Notably, on the premise of meeting the minimum reliability requirements of the safety constraints, with increasing sample size, the DR-DOPF model sacrifices reliability in exchange for higher economic benefits. It is easy to calculate that when the sample size is 2000, the comprehensive cost of DR-DOPF is only 1.5% higher and the water spillage is only 1.8% more compared to SO, which shows that when the sample is large enough, the DR-DOPF model can ensure reliability based on small economic loss. Compared with the over-conservatism of RO and the over-aggressiveness of SO, DR-DOPF can balance economy and conservatism well. The above analysis once again confirms the previous conclusion on the conservativeness ranking; i.e., in the IEEE-300 system, conservativeness is still ranked from high to low as: RO > DR-DOPF (20) > DR-DOPF (50) > DR-DOPF (200) > DR-DOPF (1000) > DR-DOPF (2000) > SO.

In addition, we also study the influence of the confidence level of the Wasserstein ambiguity set on the results. The sampling number is $N = 1000$, and the results of DR-DOPF at different confidence levels and of SO and RO are obtained. The results are displayed in Figure 8.

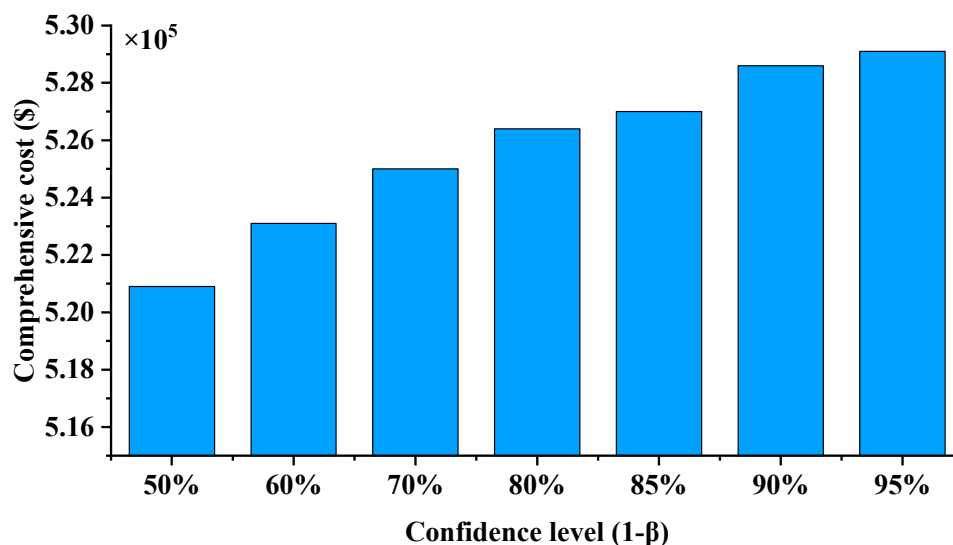


Figure 8. Comprehensive cost with confidence level.

Figure 8 shows that the comprehensive cost increases with the confidence level, because when the confidence level increases, to ensure that the ambiguity set contains the real distribution with a higher probability, the Wasserstein radius must become larger. Therefore, the extreme distribution contained in the ambiguity set deviates from the real distribution, and the corresponding result becomes more conservative; consequently, the comprehensive generation cost increases. Hence, controlling the confidence level can limit the conservativeness of the results and ensure a balance between conservativeness and economy in the model.

5. Conclusions

In this study, a robust multi-energy dynamic distribution optimal power flow model is proposed. The model uses the ambiguity set with the Wasserstein metric to address the uncertainty of wind and solar output, and also considers water spillage. The Wasserstein ambiguity set is data-driven and does not require an assumption of the distribution information in advance. Regarding the worst-case expectation in the objective function, its exact equivalent form is obtained through reformulation. The equivalent form is highly concise, and its scale does not change with an increasing number of samples; therefore, it exhibits excellent computational performance. Further, the distributed robust chance constraints are transformed into tractable reformulations. By the above means, a tractable DR-DOPF model is proposed. By minimizing the comprehensive power generation cost, the DR-DOPF model provides the factor coefficients of each power plant participating in the regulation process during real-time dispatching. The test results of IEEE-300 and other systems indicate that, if the power system operates according to the day-ahead scheduling and regulates based on participation factors given by the DR-DOPF model, the comprehensive operation cost and water spillage of hydropower stations can be effectively reduced. In addition, with an increased sample size, the DR-DOPF model can reduce conservatism and improve economy based on satisfying the reliability of safety constraints.

Author Contributions: Conceptualization, H.W.; methodology, G.S.; software, G.S.; validation, H.W.; formal analysis, H.W. and G.S.; investigation, H.W. and G.S.; resources, H.W.; data curation, G.S.; writing—original draft preparation, G.S.; writing—review and editing, H.W. and G.S.; visualization, G.S.; supervision, H.W.; project administration, H.W.; funding acquisition, H.W. All authors have read and agreed to the published version of the manuscript.

Funding: This research was funded by the National Natural Science Foundation of China, Research on minimum water spillage mechanism of multi-energy power system based on big data driven distributed robust optimization (Funding number: 51967002).

Institutional Review Board Statement: Not applicable.

Informed Consent Statement: Not applicable.

Data Availability Statement: Not applicable.

Conflicts of Interest: The authors declare no conflict of interest.

Appendix A

Proof of Lemma 1. The optimization variables in problem (22) are κ and η , and the control variable α is equivalent to a parameter here. Let $\psi = \sum_{i \in G} \sum_{t \in T} \alpha_{i,t} d_i$, and problem (22) can be rewritten as:

$$\inf_{\kappa \geq 0} \kappa \delta + \frac{1}{N} \sum_{i=1}^N \eta_i \quad (\text{A1a})$$

$$\text{s.t. } \eta_i \geq \psi \bar{\xi} - \kappa (\bar{\xi} - \hat{\xi}_i), \forall i \leq N \quad (\text{A1b})$$

$$\eta_i \geq -\psi \underline{\xi} + \kappa (\underline{\xi} - \hat{\xi}_i), \forall i \leq N \quad (\text{A1c})$$

$$\eta_i \geq \psi |\hat{\xi}_i|, \forall i \leq N \quad (\text{A1d})$$

Because κ is a scalar, the discussion of κ is simple. Specifically, the optimal solution of problem (A1) can be obtained either in $\kappa > \psi$ or $0 \leq \kappa \leq \psi$. First, the optimal solution of the problem must not be obtained at $\kappa > \psi$. The proof is as follows:

For $\kappa \geq \psi$, the right side of Equation (A1b) is equal to:

$$\psi \bar{\xi} - \kappa (\bar{\xi} - \hat{\xi}_i) = (\psi - \kappa) (\bar{\xi} - \hat{\xi}_i) + \psi \hat{\xi}_i \leq \psi \hat{\xi}_i \leq \psi |\hat{\xi}_i| \quad (\text{A2})$$

The right side of Equation (A1c) minus $\psi |\hat{\xi}_i|$ equals the following:

$$-\psi \underline{\xi} + \kappa (\underline{\xi} - \hat{\xi}_i) - \psi |\hat{\xi}_i| = \begin{cases} (\kappa - \psi) \underline{\xi} - (\kappa + \psi) \hat{\xi}_i < 0, \hat{\xi}_i \geq 0 \\ (\kappa - \psi) (\underline{\xi} - \hat{\xi}_i) < 0, \hat{\xi}_i < 0 \end{cases} \quad (\text{A3})$$

Therefore, the right side of Equation (A1c) is also less than $\psi |\hat{\xi}_i|$.

Hence, constraints (A1b–d) can be combined, which is equivalent to constraint (A1d). To minimize the objective function, η_i must take its minimum value $\psi |\hat{\xi}_i|$. After further analysis, for $\kappa \geq \psi$, the first term $\kappa \delta$ in the objective function increases with κ , while the second term $\frac{1}{N} \sum_{i=1}^N \eta_i = \frac{1}{N} \sum_{i=1}^N \psi |\hat{\xi}_i|$ and remains unchanged. Hence, the total objective function value increases with κ . Thus, when $\kappa > \psi$, the objective function is greater than when $\kappa = \psi$. In other words, the original problem cannot yield the optimal solution for $\kappa > \psi$. Accordingly, the optimal solution must be obtained on the complement of $\kappa > \psi$, namely, $0 \leq \kappa \leq \psi$.

Because problem (A1) is a linear programming problem about κ and η , the optimal solution must be at the vertices, i.e., $\kappa = 0$ or $\kappa = \psi$. This is analyzed in the two cases below.

For $\kappa = 0$, problem (A1) is simplified as:

$$\inf_{\eta} \left\{ \frac{1}{N} \sum_{i=1}^N \eta_i \mid \eta_i \geq \psi \bar{\xi}, \eta_i \geq -\psi \underline{\xi}, \eta_i \geq \psi |\hat{\xi}_i| \right\} = \max \left\{ \psi \bar{\xi}, -\psi \underline{\xi} \right\} \quad (\text{A4})$$

For $\kappa = \psi$, problem (A1) is simplified as:

$$\inf_{\eta} \left\{ \psi \delta + \frac{1}{N} \sum_{i=1}^N \eta_i \mid \eta_i \geq \psi \hat{\xi}_i, \eta_i \geq -\psi \hat{\xi}_i, \eta_i \geq \psi |\hat{\xi}_i| \right\} = \psi \left(\delta + \frac{1}{N} \sum_{i=1}^N |\hat{\xi}_i| \right) \quad (\text{A5})$$

Therefore, the optimal value of the original problem is the smaller value of the above two cases, namely:

$$\min \left\{ \max \left\{ \psi_{\underline{\zeta}}, -\psi_{\underline{\zeta}} \right\}, \psi \left(\delta + \frac{1}{N} \sum_{i=1}^N |\hat{\zeta}_k| \right) \right\} = \min \left\{ \max \left\{ \bar{\zeta}, -\underline{\zeta} \right\}, \delta + \frac{1}{N} \sum_{i=1}^N |\hat{\zeta}_k| \right\} \cdot \psi = b\psi \tag{A6}$$

As such, the complete proof is provided. □

Appendix B

Table A1. Parameters of hydropower stations.

Hydropower Station	Connection Node	r_i^{ini} ($\times 10^4$ m ³)	r_i^{fin} ($\times 10^4$ m ³)	r_i^h ($\times 10^4$ m ³)	\bar{r}_i^h ($\times 10^4$ m ³)	\underline{P}_i^h (MW)	\bar{P}_i^h (MW)
H1	78	4500	4500	4000	4900	45.90	232.56
H2	34	21,600	21,600	21,000	22,000	90.44	445.74
H3	92	8600	8600	5500	9000	58.80	318.30

H1: Bapanxia Hydropower Station; H2: Yanguoxia Hydropower Station; H3: Daxia Hydropower Station.

Table A2. Parameters of hydropower stations.

Hydropower Station	$k_{i,1}$ (MW·s/m ³)	$k_{i,2}$ (MW·s/m ³)	$k_{i,3}$ (MW·s/m ³)	$k_{i,4}$ (MW·s/m ³)	$\underline{q}_{i,m}$ (m ³ /s)	$\bar{q}_{i,m}$ (m ³ /s)	\bar{q}_i (m ³ /s)
H2	0.145	0.161	0.145	0.161	300	305	1520
H1	0.315	0.331	0.315	0.331	280	275	1380
H3	0.188	0.204	0.188	0.204	300	331	1624

Table A3. Parameters of wind and solar output data.

Time	P^w (MW)	P^s (MW)	\bar{P}^w (MW)	\bar{P}^s (MW)	Time	P^w (MW)	P^s (MW)	\bar{P}^w (MW)	\bar{P}^s (MW)
1	310.2	0	269.3	0	13	176.1	129.6	202.1	191.8
2	271.3	0	231.4	0	14	145.4	123.8	135.5	145.1
3	263.3	0	263.7	0	15	154	101.5	264.8	179.6
4	214.8	0	258.4	0	16	141.1	85.7	303.9	171.4
5	190.7	0	357.8	0	17	158.6	58.8	370	105
6	171.4	0	403	0	18	168.7	24.3	345.1	45.2
7	192.7	5.1	451.7	10.2	19	229.8	4.9	344.7	9.8
8	203.6	14.8	413.2	5	20	314.9	0	318.4	0
9	190.6	34.4	362.1	54.8	21	315.2	0	285.6	0
10	165	75.3	178.9	66.3	22	370.8	0	335.3	0
11	176.1	90.3	130.4	102.7	23	390	0	400.7	0
12	179.8	120.6	166	144.5	24	406.1	0	374.6	0

P^w : Forecasting wind power; P^s : Forecasting solar power; \bar{P}^w : Real wind power; \bar{P}^s : Real solar power.

References

1. National Energy Administration. *Implementation Plan for Solving the Problem of Spillage Water, Air and Light*; National Energy Administration: Beijing, China, 2017.
2. Shaheen, A.M.; Elsayed, A.M.; El-Sehiemy, R.A.; Ghoneim, S.S.; Alharthi, M.M.; Ginidi, A.R. Multi-dimensional energy management based on an optimal power flow model using an improved quasi-reflection jellyfish optimization algorithm. *Eng. Optim.* **2022**, *1*–23. [[CrossRef](#)]
3. El-Sehiemy, R.; Elsayed, A.; Shaheen, A.; Elattar, E.; Ginidi, A. Scheduling of Generation Stations, OLTC Substation Transformers and VAR Sources for Sustainable Power System Operation Using SNS Optimizer. *Sustainability* **2021**, *13*, 11947. [[CrossRef](#)]
4. Shaheen, A.M.; El-Sehiemy, R.A.; Hasanien, H.M.; Ginidi, A.R. An improved heap optimization algorithm for efficient energy management based optimal power flow model. *Energy* **2022**, *250*, 123795. [[CrossRef](#)]
5. Shaheen, A.M.; El-Sehiemy, R.A.; Alharthi, M.M.; Ghoneim, S.S.; Ginidi, A.R. Multi-objective jellyfish search optimizer for efficient power system operation based on multi-dimensional OPF framework. *Energy* **2021**, *237*, 121478. [[CrossRef](#)]
6. Achiluzzi, E.; Kobikrishna, K.; Sivabalan, A.; Sabillon, C.; Venkatesh, B. Optimal asset planning for prosumers considering energy storage and photovoltaic (PV) units: A stochastic approach. *Energies* **2020**, *13*, 1813. [[CrossRef](#)]
7. Zheng, Q.P.; Wang, J.; Liu, A.L. Stochastic optimization for unit commitment—A review. *IEEE Trans. Power Syst.* **2014**, *30*, 1913–1924. [[CrossRef](#)]

8. Agabalaye-Rahvar, M.; Mansour-Saatloo, A.; Mirzaei, M.A.; Mohammadi-Ivatloo, B.; Zare, K.; Anvari-Moghaddam, A. Robust optimal operation strategy for a hybrid energy system based on gas-fired unit, power-to-gas facility and wind power in energy markets. *Energies* **2020**, *13*, 6131. [[CrossRef](#)]
9. Bai, X.; Qu, L.; Qiao, W. Robust AC optimal power flow for power networks with wind power generation. *IEEE Trans. Power Syst.* **2015**, *31*, 4163–4164. [[CrossRef](#)]
10. Lorca, A.; Sun, X.A. Multistage robust unit commitment with dynamic uncertainty sets and energy storage. *IEEE Trans. Power Syst.* **2016**, *32*, 1678–1688. [[CrossRef](#)]
11. Han, S.; Kim, H.-J.; Lee, D. A Long-Term Evaluation on Transmission Line Expansion Planning with Multistage Stochastic Programming. *Energies* **2020**, *13*, 1899. [[CrossRef](#)]
12. Ren, J.; Xu, Y.; Wang, S. A Distributed Robust Dispatch Approach for Interconnected Systems with a High Proportion of Wind Power Penetration. *Energies* **2018**, *11*, 835. [[CrossRef](#)]
13. Zhao, C.; Jiang, R. Distributionally robust contingency-constrained unit commitment. *IEEE Trans. Power Syst.* **2017**, *33*, 94–102. [[CrossRef](#)]
14. Jabr, R.A. Distributionally robust CVaR constraints for power flow optimization. *IEEE Trans. Power Syst.* **2020**, *35*, 3764–3773. [[CrossRef](#)]
15. Wang, Z.; Bian, Q.; Xin, H.; Gan, D. A distributionally robust co-ordinated reserve scheduling model considering CVaR-based wind power reserve requirements. *IEEE Trans. Sustain. Energy* **2015**, *7*, 625–636. [[CrossRef](#)]
16. Mohajerin Esfahani, P.; Kuhn, D. Data-driven distributionally robust optimization using the Wasserstein metric: Performance guarantees and tractable reformulations. *Math. Program.* **2018**, *171*, 115–166. [[CrossRef](#)]
17. Yang, I. Data-driven distributionally robust stochastic control of energy storage for wind power ramp management using the Wasserstein metric. *Energies* **2019**, *12*, 4577. [[CrossRef](#)]
18. Duan, C.; Fang, W.; Jiang, L.; Yao, L.; Liu, J. Distributionally robust chance-constrained approximate AC-OPF with Wasserstein metric. *IEEE Trans. Power Syst.* **2018**, *33*, 4924–4936. [[CrossRef](#)]
19. Zhu, R.; Wei, H.; Bai, X. Wasserstein metric based distributionally robust approximate framework for unit commitment. *IEEE Trans. Power Syst.* **2019**, *34*, 2991–3001. [[CrossRef](#)]
20. Zhou, A.; Yang, M.; Wang, M.; Zhang, Y. A linear programming approximation of distributionally robust chance-constrained dispatch with Wasserstein distance. *IEEE Trans. Power Syst.* **2020**, *35*, 3366–3377. [[CrossRef](#)]
21. Liu, H.; Fan, Z.; Xie, H.; Wang, N. Distributionally Robust Joint Chance-Constrained Dispatch for Electricity-Gas-Heat Integrated Energy System Considering Wind Uncertainty. *Energies* **2022**, *15*, 1796. [[CrossRef](#)]
22. Yang, J.; Zhang, N.; Kang, C.; Xia, Q. A state-independent linear power flow model with accurate estimation of voltage magnitude. *IEEE Trans. Power Syst.* **2016**, *32*, 3607–3617. [[CrossRef](#)]
23. Wu, L. A tighter piecewise linear approximation of quadratic cost curves for unit commitment problems. *IEEE Trans. Power Syst.* **2011**, *26*, 2581–2583. [[CrossRef](#)]
24. Wang, M.F.; Au, F. Precise integration methods based on Lagrange piecewise interpolation polynomials. *Int. J. Numer. Methods Eng.* **2010**, *77*, 998–1014. [[CrossRef](#)]
25. Liu, B.; Zhang, Q.; Ge, X.; Yuan, Z. CVaR-based approximations of Wasserstein distributionally robust chance constraints with application to process scheduling. *Ind. Eng. Chem. Res.* **2020**, *59*, 9562–9574. [[CrossRef](#)]
26. Yan, J.; Li, K.; Bai, E.W.; Deng, J.; Foley, A.M. Hybrid probabilistic wind power forecasting using temporally local Gaussian process. *IEEE Trans. Sustain. Energy* **2015**, *7*, 87–95. [[CrossRef](#)]
27. Zhang, J.; Yan, J.; Infield, D.; Liu, Y.; Lien, F.S. Short-term forecasting and uncertainty analysis of wind turbine power based on long short-term memory network and Gaussian mixture model. *Appl. Energy* **2019**, *241*, 229–244. [[CrossRef](#)]
28. Yuan, T.I.A.N.; Keyou, W.A.N.G.; Guojie, L.; Weichun, G.; Huanhuan, L. Dynamic stochastic optimal power flow based on second-order cone programming considering wind power correlation. *Autom. Electr. Power Syst.* **2018**, *42*, 41–47.
29. Lee, D.; Baldick, R. Probabilistic wind power forecasting based on the laplace distribution and golden search. In Proceedings of the 2016 IEEE/PES Transmission and Distribution Conference and Exposition (T&D), Dallas, TX, USA, 2–4 May 2016; IEEE: Piscataway, NJ, USA, 2016.
30. Wang, Z.; Shen, C.; Liu, F.; Wu, X.; Liu, C.C.; Gao, F. Chance-constrained economic dispatch with non-Gaussian correlated wind power uncertainty. *IEEE Trans. Power Syst.* **2017**, *32*, 4880–4893. [[CrossRef](#)]